Received: 12 May 2023 | Revised: 24 October 2023 | Accepted: 26 October 2023

https://doi.org/10.1016/j.jtha.2023.10.025

ORIGINAL ARTICLE

Interplay of fibrinogen α_EC globular domains and factor XIIIa cross-linking dictates the extensibility and strain stiffening of fibrin networks

Cristina Martinez-Torres[1,2] | Jos Grimbergen[3] | Jaap Koopman[3] | Gijsje H. Koenderink[1,2]

[1]AMOLF, Amsterdam, The Netherlands

[2]Department of Bionanoscience, Kavli Institute of Nanoscience Delft, Delft University of Technology, Delft, The Netherlands

[3]Fibriant B.V., Leiden, The Netherlands

Correspondence
Gijsje H. Koenderink, Department of Bionanoscience, Kavli Institute of Nanoscience Delft, Delft University of Technology, Van der Maasweg 9, 2629 HZ Delft, The Netherlands.
Email: g.h.koenderink@tudelft.nl

Present address
Cristina Martinez-Torres, Institute of Physics and Astronomy, University of Potsdam, 28, Karl-Liebknecht-Straße 24/25, Potsdam 14476, Germany.

Funding information
C.M.-T. gratefully acknowledges financial support via a VENI grant from the Netherlands Organization for Scientific Research (grant number 680-47-462). This work was supported by funding from the European Union's Horizon Europe Research and Innovation Program (under grant agreement number 190183175) and research funding provided by Fibriant B.V.

Abstract

Background: Fibrinogen is a plasma protein forming the fibrin scaffold of blood clots. Its mechanical properties therefore affect the risk of bleeding as well as thrombosis. There has been much recent interest in the biophysical mechanisms controlling fibrin mechanics; however, the role of molecular heterogeneity of the circulating fibrinogen in determining clot mechanical function remains poorly characterized.

Objectives: By comparing 2 fibrinogen variants where the only difference is the Aα-chain length, with one variant having a globular domain at its C-terminus, this study aimed to reveal how the molecular structure impacts the structure and mechanics of fibrin networks.

Methods: We characterized the mechanical response to large shear for networks formed from 2 recombinant fibrinogen variants: the most prevalent variant in circulation with a molecular weight of 340 kDa (recombinant human fibrinogen [rFib] 340) and a minor variant with a molecular weight of 420 kDa (rFib420).

Results: We show that the elastic properties of the 2 variants are identical when fibrin is cross-linked with factor XIIIa but differ strongly in its absence. Uncross-linked rFib420 networks are softer and up to 3-fold more extensible than rFib340 networks. Electron microscopy imaging showed that the 2 variants formed networks with a comparable structure, except at 4 mg/mL, where rFib420 formed denser networks.

Conclusion: We propose that the α_EC domains of rFib420 increase the extensibility of uncross-linked fibrin networks by promoting protofibril sliding, which is blocked by FXIIIa cross-linking. Our findings can help explain the functional role of different circulating fibrinogen variants in blood clot mechanics and tissue repair.

KEYWORDS
blood coagulation, elasticity, electron microscopy, fibrin, rheology

Manuscript handled by: Ton Lisman

Final decision: Ton Lisman, 26 October 2023

1 | INTRODUCTION

Fibrin networks form the mechanical backbone of blood clots, providing high extensibility under shear and tensile deformations [1]. Moreover, fibrin networks strongly strain-stiffen and thus strengthen blood clots against stresses exerted by blood flow, muscle activity, and various cells, which is important to prevent bleeding and thromboembolism [2,3].

This remarkable nonlinear mechanical behavior of fibrin is a consequence of its hierarchical structure, which forms via stepwise self-assembly. Human plasma contains a soluble precursor protein known as fibrinogen at a typical concentration of 2 to 3 mg/mL [4]. Fibrinogen consists of 2 sets of 3 polypeptide chains, Aα, Bβ, and γ, which fold into a trinodular structure with a central E-nodule and 2 distal D-nodules, separated by coiled connectors (Figure 1A) [5]. The Aα-chains are distinct from the Bβ and γ chains because they terminate in long and unstructured carboxy-terminal regions, the αC-regions, that form flexible loops emanating from the coiled-coils [6,7]. Thrombin triggers fibrin network formation by enzymatically converting fibrinogen to fibrin, exposing complementary interaction sites on the D- and E-nodules that drive self-assembly into half-staggered pairs of linear strands, known as protofibrils (Figure 1B) [8]. These protofibrils grow both longitudinally and laterally, forming thick fibers composed of tens of protofibrils, as measured by turbidimetry and single-molecule imaging [9–11]. The fibers branch into a random network structure whose pore size and junction topology depend on the environmental conditions and on the protein concentrations [12,13]. The fibrin network is further stabilized by the action of factor XIIIa (FXIIIa), a transglutaminase that creates covalent γ-glutamyl-ϵ-lysinyl isopeptide bonds between reactive glutamines and lysines in the γ-chains and at multiple sites in the αC region [14,15].

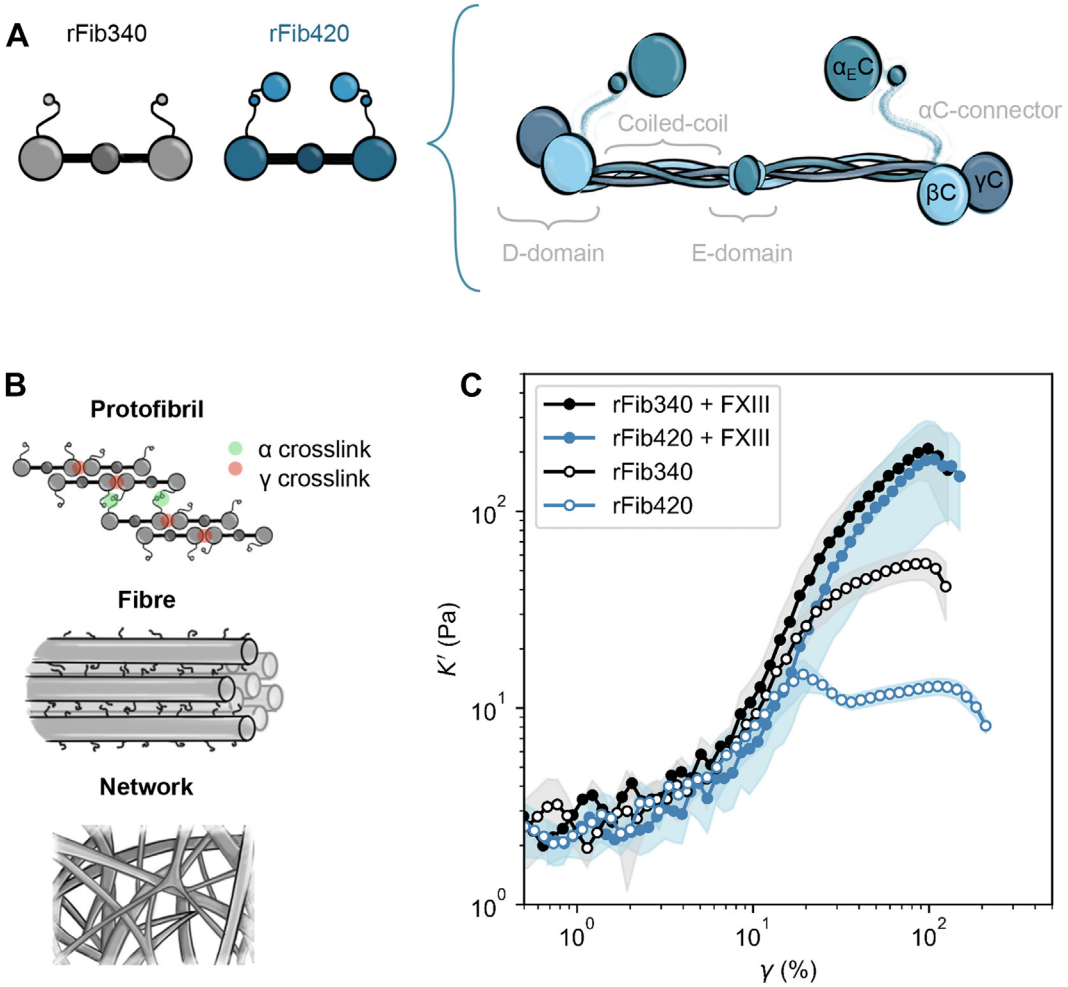

FIGURE 1 Strain stiffening of recombinant human fibrinogen (rFib) 340 and rFib420 fibrin networks under shear loading. (A) Schematic representation of the rFib340 (in gray) and rFib420 (in blue) fibrinogen molecules, showing their characteristic trinodular structure with the D- and E-globular domains, the flexible unstructured αC-connectors, and the folded αC-terminal domains. rFib420 differs from rFib340 only in the presence of a C-terminal 236-residue extension of the α-chain, which forms a globular α_EC domain that resembles the βC and γC domains. (B) Scheme of the different structural levels of fibrin assembly. The α–α and γ–γ cross-links mediated by factor XIIIa are shown at the protofibril level. (C) Differential elastic modulus (K') as a function of applied shear strain (γ) for rFib340 and rFib420 networks (both 1 mg/mL) with and without FXIIIa (see legend). The solid lines indicate the mean curves from 3 independent measurements, and the shading represents the SD. The last data point in each curve is taken just before network rupture.

Human plasma of healthy individuals contains many different variants of the fibrinogen molecule. The abundance of some of these molecular variants changes with human age and disease status [16,17]. Fibrinogen is synthesized in the liver in a high-molecular-weight form (molecular weight [MW], 340 kDa), which constitutes approximately 70% of the total fibrinogen in the circulation. Partial degradation of the carboxy-terminus of the fibrinogen Aα-chain (αC) results in 2 low-molecular-weight forms with either one of the Aα-chains degraded (MW, 305 kDa; approximately 26% of total fibrinogen) or both Aα-chains degraded (MW, 270 kDa; approximately 4% of total fibrinogen) [17–19]. Comparative studies of high-molecular-weight fibrinogen and the low-molecular-weight variants purified from human plasma or αC-truncated recombinant variants showed that they differ in coagulation rate, fibrin network structure, and fibrin–endothelial cell interactions [18,20–23]. In addition, 2 splice variants are present in circulation. One splice variant has an extended α-chain resulting in a MW of 420 kDa (fibrinogen-420), while the other splice variant has a modification at the C-terminus of the γ-chain (γ′-fibrinogen) [24]. Fibrinogen-420 constitutes approximately 1% to 3% of the total fibrinogen pool in human plasma and is more highly expressed in newborns than in adults [16], reflecting unidentified but potentially important functions. This variant is identical to the more abundant fibrinogen-340 variant, except for an additional stretch of 236 residues at the C-terminus of both Aα-chains that forms a globular domain known as the α_EC domain (Figure 1A). This domain shares structural and sequence homology with the fibrinogen βC and γC domains [25,26] and is highly conserved across the vertebrate kingdom [27]. In human fibrinogen, it is the only known region of the α-chain to be glycosylated [28]. The α_EC domain lacks a fibrin polymerization pocket and does not interact with the rest of the molecule [29]. Nevertheless, electron microscopy and turbidity data suggest that it hampers lateral association of protofibrils because fibrinogen-420 forms clots with a higher branching density and thinner fibers than fibrinogen-340 [30].

Currently, little is known about the physiological role of fibrinogen-420 and its α_EC domain. It has been speculated that the function of the α_EC domain is independent of the fibrinogen molecule, given that plasmin-mediated degradation of fibrin(ogen)-420 releases the α_EC domain as a stable cleavage product with chaperone activity [31,32]. Yet it is possible that the α_EC domain affects the mechanical properties of fibrin networks since the αC-region is known to strongly affect fibrin network extensibility. The majority of the αC-region is intrinsically disordered (residues 221 to 391) and, therefore, forms long and flexible chains that interconnect the much stiffer protofibrils [7]. Theoretical models predict that, depending on the length and molecular connectivity of the protofibrils, the αC-regions can facilitate force-induced fiber elongation through protofibril sliding [33]. This prediction is supported by mechanical measurements on single fibrin fibers [34] and on networks thereof [35–37].

Here, we perform a direct biophysical comparison between fibrin networks made from recombinant human fibrinogen (rFib) 420 vs fibrinogen-340. By using recombinant fibrinogen variants, we ensured molecularly homogeneous systems of a single fibrinogen variant without any contaminants often present in plasma-derived fibrinogen. Plasma-derived fibrinogen preparations are heterogeneous due to proteolytic degradation and alternative splicing as mentioned above, heterogeneity in posttranslational fibrinogen modifications, and the presence of contaminants such as FXIII and fibronectin [18,24,25,38,39]. We focus on the mechanical response of reconstituted fibrin networks to large shear deformations in order to unveil the role of the α_EC domain of the fibrinogen 420 variant in the strain-stiffening behavior of fibrin. By comparing the mechanical behavior and structure of fibrin networks made of the fibrinogen 420 and 340 variants, we disentangled the contributions of protofibril sliding and FXIIIa-mediated cross-linking to fibrin network extensibility.

2 | MATERIALS AND METHODS

2.1 | Sample preparation

rFib with α-chains having a length of 610 amino acids, corresponding to the main constituent of plasma fibrinogen (rFib340), and recombinant fibrinogen with α-chains of length of 847 amino acids (rFib420), corresponding to the α-extended variant of plasma fibrinogen, were expressed in mammalian cells and purified from cell culture supernatant according to a published procedure [11]. The proteins were stored in phosphate-buffered saline (8.65-mM Na_2HPO_4, 1.92-mM NaH_2PO_4, and 140-mM NaCl at pH 7.4) at −80 °C at stock concentrations of 14.94 mg/mL (rFib340) and 16.7 mg/mL (rFib420). Human α-thrombin was purchased as a lyophilized powder from Enzyme Research Laboratories and reconstituted in water according to the manufacturer's instructions to obtain a 1000 NIH U/mL stock solution in 50-mM sodium citrate and 0.2-M NaCl at pH 6.5. Aliquots were snap-frozen in liquid nitrogen and stored at −80 °C. Human FXIII was purchased in zymogen form (Enzyme Research Laboratories) and stored at −80 °C at a stock concentration of 8000 IU/mL in 50-mM Tris, 100-mM NaCl, 1-mM EDTA, 10-U/mL aprotinin, and 20% glycerol, pH 7.5.

Fibrin networks were prepared by mixing the recombinant fibrinogens with 0.5 NIH U/mL α-thrombin and incubating for 45 minutes at 37 °C in fibrin polymerization buffer containing 20-mM 4-(2-hydroxyethyl)-1-piperazineethanesulfonic acid (HEPES) at pH 7.4, 150-mM NaCl, and 5-mM $CaCl_2$. Before the addition of thrombin, fibrinogen samples diluted with fibrin polymerization buffer were first incubated for 10 minutes at room temperature to allow for Ca^{2+} binding to fibrinogen. To obtain covalently cross-linked networks, FXIII was first diluted in fibrin polymerization buffer and added as 10% v/v of the total volume to a final concentration of 3 IU/mL, and networks were left to polymerize for 90 minutes at 37 °C to allow completion of cross-linking.

We characterized the purity of the fibrinogen preparations as well as the degree of FXIIIa-mediated covalent cross-linking upon fibrin assembly by denaturing polyacrylamide gel electrophoresis. After polymerization, fibrin networks were mixed with an equal volume of

2× lithium dodecyl sulfate (LDS) reducing mix supplemented with 1-M urea (NuPage LDS Sample Buffer and Sample Reducing Agent, Life Technologies, Thermo Fisher Scientific) and heated for 10 minutes at 70 °C. Samples holding the equivalent of 5 μg of fibrinogen per lane were run on 4% to 12% Bis-Tris gels (Life Technologies, Thermo Fisher Scientific). The gels were stained using InstantBlue (Expedeon) and scanned.

2.2 | Rheology

Rheological measurements were performed using 2 different stress-controlled rheometers (which gave comparable results): a Kinexus DSR instrument (Malvern Panalytical) and an MCR501 instrument (Anton Paar), both equipped with a stainless steel cone-plate geometry (20 mm diameter, 1° cone angle). Fibrin networks were polymerized in situ by transferring 40 μL of the fibrinogen solution immediately upon the addition of thrombin (and, where indicated, FXIII) onto the preheated bottom plate. Solvent evaporation was prevented by applying mineral oil (M3516, Sigma-Aldrich) around the sample edge. Fibrin network formation was monitored by applying a small oscillatory shear strain with an amplitude of 0.5% and a frequency of 0.5 Hz. The steady-state values for the linear storage (G') shear moduli were extracted by fitting the time dependencies with an exponential function (Supplementary Figure S1). Each data point represents the average of at least 2 independently prepared samples (see Supplementary Table S1 for details).

The strain-stiffening behavior of the fully polymerized fibrin networks was measured on the Kinexus rheometer by applying a logarithmic stress ramp at a rate of 200 seconds/decade to avoid any possible role of slow structural rearrangements [40]. The differential elastic modulus, K', was computed from the tangent of the applied shear stress (σ) vs the resultant strain (γ) curve: $K' = d\sigma/d\gamma$.

To test the stress-strain reversibility, we subjected the samples to a repeated large-strain loading protocol proposed by Münster et al. [41] using the MCR501 rheometer. Briefly, we imposed sinusoidal strain cycles at a fixed oscillation frequency of 0.01 Hz but with a stepwise increasing strain amplitude of 20%, starting at a strain of 20% and going up in linearly increasing steps until rupture. We recorded 10 stress-strain cycles at each strain amplitude. We analyzed the data in the same manner as originally proposed by Münster et al. [41]. To compare the stress-strain relation between cycles of fixed strain amplitude, we first quantified the shift in the onset of nonlinearity in the elastic component of the viscoelastic stress-strain relation, $\sigma_{el}(\gamma)$, which we determined by averaging the stress $\sigma(\gamma)$ measured during loading and unloading. We then chose an arbitrary threshold stress σ_{th} (35 Pa for rFib340 and 10 Pa for rFib420), that intersects all strain-stress curves with an evident shift for the consecutive cycles and calculated the characteristic strain, γ_{char}, where $\sigma_{el}(\gamma_{char})$ reached σ_{th}. Using this procedure, we obtained master curves for the full viscoelastic stress $\sigma(\gamma-\gamma_{char})$ for each cycle.

2.3 | Scanning electron microscopy

Directly after mixing fibrinogen with thrombin (and, where indicated, FXIII), 20 μL samples were transferred to Petri dishes with a glass-bottom well (CellVis, IBL Baustoff + Labor GmbH). The samples were placed in the center of the well to avoid contact with the side walls and to facilitate gentle fluid exchanges during further sample preparation. Dehydration was prevented by placing a wet tissue within the Petri dish and sealing it with parafilm on the outside. After polymerization (90 minutes at 37 °C), the fibrin networks were washed 3 times for 10 minutes each with either sodium cacodylate buffer (50 mM cacodylate, 150 mM NaCl, pH 7.4) or fibrin polymerization buffer (both buffers have identical results). The networks were fixed for 2 hours with 2.5% glutaraldehyde in sodium cacodylate or fibrin polymerization buffer and washed again 3 times for 10 minutes each in the buffer. The samples were then dehydrated by a series of graded ethanol, immersed in HDMS (hexamethyldisilazane, Sigma-Aldrich), and air-dried. The resulting thin films were mounted upside down on a support with carbon tape (Ted Pella), sputter-coated (Leica; EM ACE600) with a 12-nm layer of palladium gold, and imaged with a scanning electron microscope (Verios 460, FEI). Images for analysis were taken at random locations, at a magnification of 100 000× (field of view approximately 4 μm wide). For 1 mg/mL networks (cross-linked and uncross-linked), we analyzed 25 images from 1 sample for each variant. For uncross-linked 2 mg/mL networks, we analyzed 11 images from 2 samples (rFib340) and 13 images from 2 samples (rFib420). For uncross-linked 4 mg/mL networks, we analyzed 14 images from 1 sample (rFib340) and 9 images from 1 sample (rFib420).

The diameter of the fibrin fibers was measured from scanning electron microscopy (SEM) images using an automated method in ImageJ [42]. The images were first processed with a double-band pass filter to filter out noise (filter size, 3 pixels) and large-scale intensity variations (filter size, 20 pixels). Then, the images were analyzed with the "Local thickness" function. Since the sample preparation for SEM anyhow tends to change the fiber diameter due to drying and metal-coating, we only used the diameter as a relative measurement to compare different networks. We also independently measured fiber diameters by scanning transmission electron microscopy (STEM) (see below). The computed thickness values were finally processed with a custom-written Python script to obtain fiber diameter distributions for each image.

The quantification of network branching was performed by manually classifying regions of interest containing network junctions (see details in Supplementary Methods). The reported results were obtained from at least 5 different sample locations chosen at random. We typically observed 10 to 30 junctions per image and gathered data from 10 to 25 images per sample and 1 or 2 samples per condition.

2.4 | STEM

Fibrin networks were formed at 1 mg/mL, similar to the samples for SEM. After polymerization, the gel drops were split by carefully

touching their surface with a glass coverslip for 10 seconds to allow for fibrin attachment and subsequently removing the coverslip to break the network. Next, electron microscopy grids with a copper mesh and thin carbon coating (5-10 nm; Ted Pella) were put in contact for 30 seconds with the newly exposed surface of the gel from either the Petri dish or the coverslip side. This transfer method ensured that the network was assembled in the same conditions as for SEM and rheology measurements while providing a quasi-2-dimensional layer compatible with transmission imaging. We chose to peel off a layer from the internal part of the drop to avoid any artifacts from the fibrin film known to form at the gel-glass and gel-air interface [43]. The samples on the grids were rinsed 5 times with Milli-Q water. To achieve quantitative molecular mass determination, we used *Tobacco mosaic virus* (TMV) rods (kindly provided by Jean-Luc Pellequer) as an internal mass calibration standard. After the final washing step, a 2 μL drop of TMV solution (25 μg/mL in phosphate-buffered saline) was added to all samples. The TMV rods were allowed to adsorb onto the grids for 1 minute at room temperature, rinsed 3 times with Milli-Q water, and blotted dry. Before imaging, the samples were air-dried at 37 °C for 10 minutes.

Imaging was performed within 2 hours after sample preparation, using the high-angle annular dark-field mode on a Verios 460 electron microscope (FEI), with an electron dose below 1000 e^-/nm^2. With this technique, we collected only those electrons that were scattered at very high angles, resulting in images where the intensity in each pixel was proportional to the local mass of the specimen [44]. To retrieve the mass per length of the fibers with high throughput, we used a semiautomated tracking algorithm that analyzes the transverse intensity profiles and the diameter all along the fiber axis (approximately one transverse profile per pixel, with 1 pixel measuring around 2 nm) described in the study by Martinez-Torres et al. [45] and publicly available on GitHub.

3 | RESULTS

3.1 | Fibrin network strain stiffening

Fibrin networks strain-stiffen and withstand large strains before breakage [1]. The strain-stiffening response comprises a small-strain regime where fibrin fibers are straightened and aligned along the principal direction of strain, followed by a high-strain regime where the fiber backbones experience tensile strain [35,46,47]. We hypothesized that any mechanical effects of the α_EC domain present in the rFib420 variant but not in the rFib340 variant (Figure 1A) should be most noticeable at high strain, where the fiber backbone is directly loaded. To test this hypothesis, we compared the mechanical response of fibrin networks formed from the 2 variants by applying a steadily increasing shear stress until the networks ruptured and recorded the resultant strain. We used recombinant versions of the 2 fibrinogen variants with a purity of >99% to ensure molecularly homogeneous systems (Supplementary Figure S3).

Figure 1C shows the differential elastic moduli, K', of the fibrin networks prepared from 1 mg/mL rFib340 or rFib420 fibrinogen. Both cross-linked and uncross-linked fibrin networks showed a linear elastic regime until the strain reached approximately 10%. In the linear elastic regime, the elastic modulus G_o is dominated by the thermal bending fluctuations of the fibers [48,49]. We found no significant effect of FXIIIa on G_o (Supplementary Figure S2B and Supplementary Table S1) and no significant differences between networks of rFib340 (G_o = 3.1 ± 1.01 Pa without FXIIIa and G_o = 2.31 ± 1.05 Pa with FXIIIa) and rFib420 (G_o = 3.05 ± 0.8 Pa without FXIIIa and G_o = 3.33 ± 1.64 Pa with FXIIIa). However, when the strain was increased beyond 20%, the strain-stiffening curves started to differ strongly from each other. FXIIIa cross-linked networks made of rFib340 or rFib420 showed a nearly identical response. We noted that both variants showed a similar level of FXIIIa-mediated cross-linking (Supplementary Figure S3), consistent with previous studies [31]. However, in the absence of FXIIIa, strain stiffening was suppressed for both variants, and they showed a strikingly different response. Uncross-linked rFib340 networks still showed a weak stiffening response above strains of 20% until they ruptured at 124 ± 4% strain. Instead, uncross-linked rFib420 networks softened above strains of 20% and tolerated a much larger maximum strain (206 ± 25%) before rupturing.

To further reveal the differences in network mechanics for the 2 uncross-linked variants, we next compared their strain-stiffening behavior over a wider concentration range, from 1 to 4 mg/mL (Figure 2). We again found that the linear elastic response was similar for both variants across this entire concentration range (Figure 2A, inset). In both cases, the storage modulus (G_o) showed a quadratic dependence on the fibrinogen concentration (c), as expected for disordered fibrous networks [50]. By contrast, the 2 variants again showed a strikingly different response at large strains (Figure 2A). The rupture strain of rFib340 networks showed only a weak dependence on the fibrin concentration, reaching a maximum of around 200% at the highest concentration of 4 mg/mL. By contrast, the rupture strain of rFib420 networks strongly depended on fibrinogen concentration, increasing from 200% at 1 mg/mL to nearly 600% at 4 mg/mL (Figure 2A). In addition, the softening behavior of the rFib420 networks, visible as a bump in the strain-stiffening curve, was enhanced with increased fibrinogen concentration (open symbols in Figure 2B). Thus, rFib420 networks were always considerably softer than rFib340 networks at large strains. In contrast, FXIIIa cross-linked networks at 4 mg/mL showed an identical strain-stiffening behavior for the 2 variants (solid symbols in Figure 2B), similar to what we observed at 1 mg/mL.

Altogether, the rheology experiments revealed a clear difference between the nonlinear elastic behavior of the 2 variants, but only at high strain and in the absence of FXIIIa. The high-strain behavior is controlled by fiber stretching. Prior studies have shown that fibrin fibers can stretch by different mechanisms, including protofibril sliding [41], forced monomer unfolding [37,51,52], and straightening of the αC-linker regions [35,48,53,54]. The relative importance of these 3 mechanisms depends on the extent of cross-linking of the fibers. High levels of intermolecular cross-linking should prevent protofibril

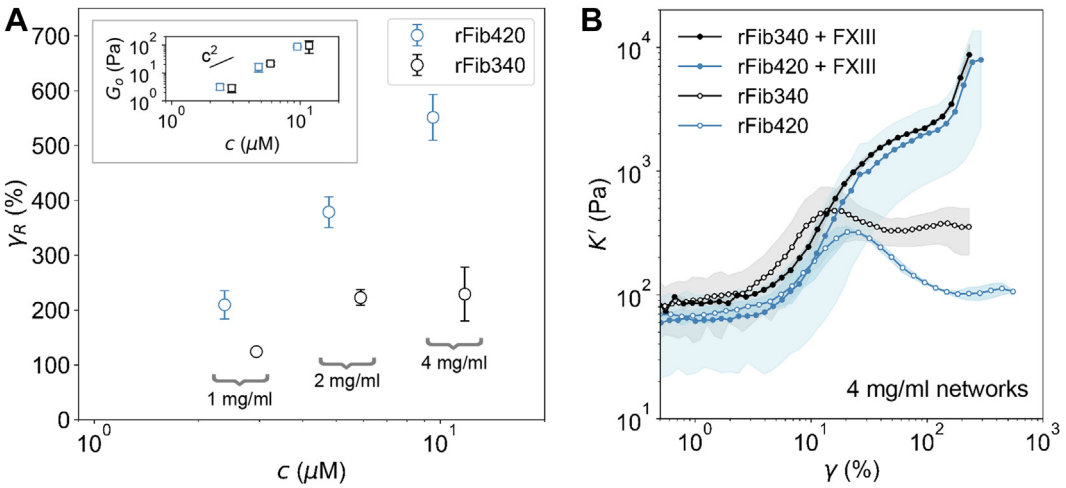

FIGURE 2 Impact of fibrinogen concentration on the strain stiffening and extensibility of recombinant human fibrinogen (rFib) 340 and rFib420 networks. (A) Mean rupture strain of uncross-linked networks, as a function of fibrinogen concentration, *c*. Inset: Mean linear storage modulus as a function of *c*. The solid line shows the c^2-scaling expected for semiflexible polymer networks. (B) The strain-stiffening curve of rFib340 and rFib420 networks at 4 mg/mL, with or without factor XIIIa. The solid lines indicate the mean curves from 2 independent measurements, and the shading represents the SD. The last point in each curve is taken just before network rupture.

sliding. For FXIIIa cross-linked networks, we therefore expect that tensile loads on the fibers can only elicit protein unfolding and/or αC-linker stretching. The only difference in the molecular structure of the 2 fibrinogen variants is the presence of the α_EC domain in rFib420. The observation that cross-linked rFib420 and rFib340 networks exhibit an identical strain-stiffening response therefore indicates that this domain does not experience any tensile load upon fiber stretching. This interpretation is consistent with structural data showing that the α_EC domains do not interact with each other and do not have any polymerization pockets [29] (Figure 1A). Alternatively, the presence of the α_EC domain could modify the fiber packing structure or the network architecture. To test whether any important structural changes occur, we next turned to electron microscopy.

3.2 | Fibrin structure

To examine the fibrin network structure for the 2 fibrinogen variants, we performed SEM, which can visualize the network connectivity, pore size, and fiber diameters (Figure 3). Representative images of rFib340 and rFib420 networks assembled at 1 mg/mL, with and without cross-linking by FXIIIa, are shown in Figure 3A. We observed no striking difference between the networks regardless of whether or not they were cross-linked (Figure 3D). However, when we raised the concentration of fibrinogen from 1 mg/mL to 4 mg/mL, more marked differences in the network structure of the 2 variants emerged (Figure 3B, Supplementary Figure S4). Uncross-linked networks at 2 mg/mL still appeared similar between the variants, but uncross-linked 4 mg/mL rFib420 networks were significantly more dense than the rFib340 networks. Accordingly, the average fiber thickness was smaller for rFib420 than for rFib340 at 4 mg/mL (Figure 3E).

As a further characterization of network structure, we compared the network connectivity for both variants by manually classifying the junction points observed in the SEM images (Figure 3C, F). At 1 mg/mL, the majority of junctions were 3-point branches. When the fibrinogen concentration was raised to 4 mg/mL, the majority of junctions (>80%) remained in the 3-point class for rFib340 networks but shifted to mainly 4+ junctions for rFib420 networks. The SEM data thus demonstrate that rFib340 and rFib420 have a similar network structure at low concentration (1 and 2 mg/mL) but differ at high concentration (4 mg/mL).

To examine the fiber structure for the 2 fibrinogen variants, we performed quantitative mass mapping with STEM. Figure 4A shows example images where the pixel intensity is proportional to the mass of the fibers. We used a semiautomated fiber tracking algorithm [45] to determine the fiber mass per unit length (MPL) and the corresponding fiber width. By plotting the MPL vs fiber width, we gain insight into the molecular packing density of the fibers, which provides a metric to characterize their structure.

For uncross-linked networks, rFib420 fibers had a significantly higher MPL than rFib340 fibers as long as the fiber width fell below approximately 300 nm (Figure 4B). For larger fiber widths, this difference disappeared, likely because the majority of the segments measured were fiber bundles. To test whether the larger MPL of rFib420 fibers was due to the higher MW of this variant or a higher packing density, we normalized the measured MPL values by the MPL of a single protofibril (14.4 kDa/nm for rFib340 and 17.8 kDa/nm for rFib420). This normalization removed the difference between the 2 variants, showing that rFib340 and rFib420 fibers of the same width consisted of the same average number of protofibrils p_f (Figure 4C). This finding indicates that the fiber packing density is comparable for both variants and is consistent with a model of fractal fiber packing

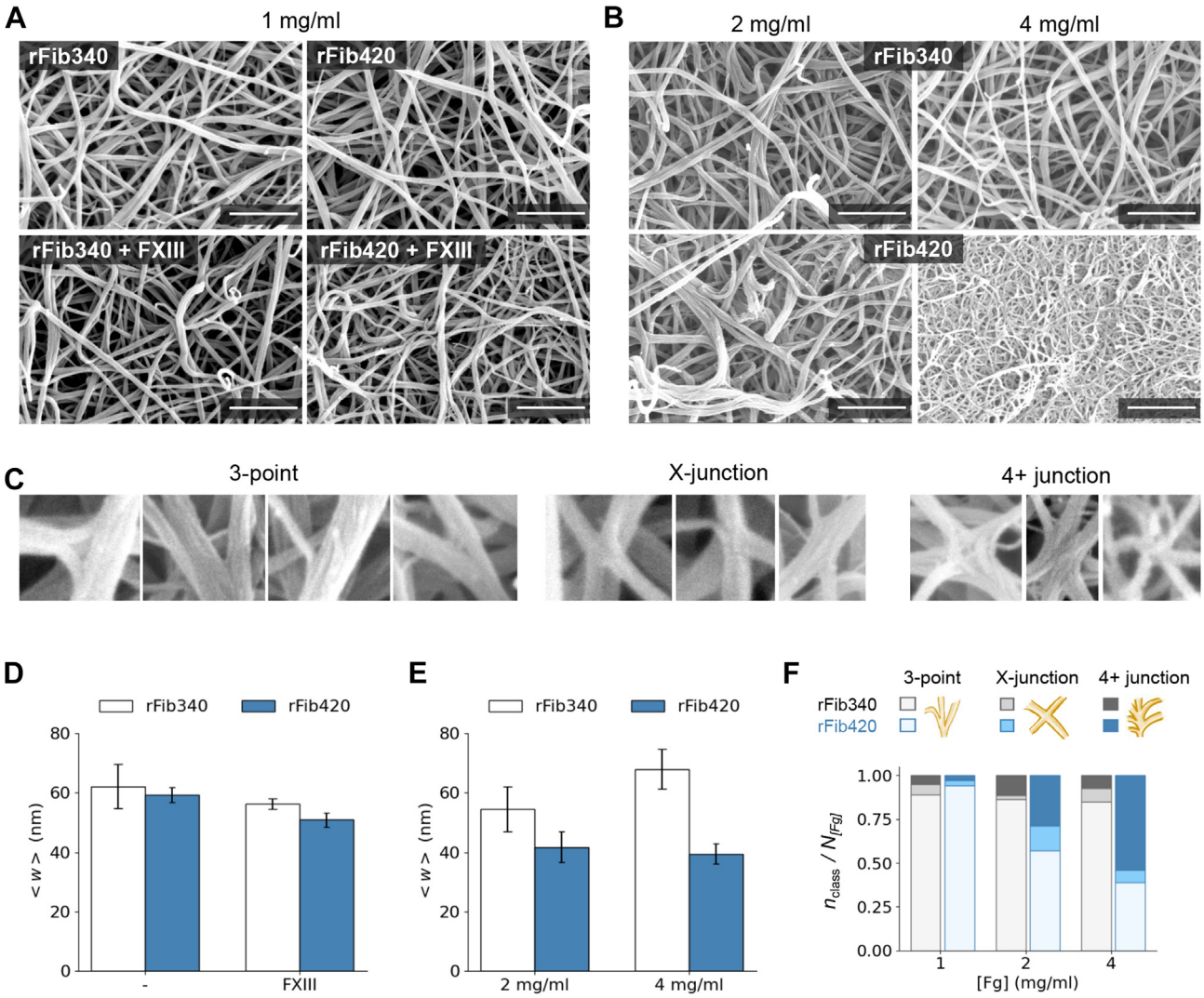

FIGURE 3 Characterization of fibrin network structure by scanning electron microscopy (SEM). (A) Representative SEM images from recombinant human fibrinogen (rFib) 340 and rFib420 networks formed at 1 mg/mL, with and without cross-linking by factor XIIIa. (B) Representative SEM images from uncross-linked rFib340 and rFib420 networks formed at 2 and 4 mg/mL. More examples can be found in the Supplementary Figure S4. Scale bar in (A, B) is 1 μm. (C) Examples of the different classes of junctions. (D, E) Quantification of fiber diameter from SEM images for rFib340 (white bars) and rFib420 (blue bars). The mean fiber diameter $< w >$ was obtained by fitting the distribution of fiber diameters within a single image. The bar height represents the mean value for (D) $n = 25$ and (E) $10 < n < 15$ images per network type, and the error bar represents the SD. (F) Quantification of different junction classes for rFib340 (gray) and rFib420 (blue) networks formed at 1, 2, and 4 mg/mL. The classes considered are sketched on the top row. The number of junctions belonging to a given class (n_{class}) is normalized by the total number per concentration and fibrinogen type ($N_{[Fg]}$).

[55], where the core is more densely packed than the periphery. FXIIIa-mediated cross-linking strongly increased the fiber packing density for both fibrinogen variants: fibers with widths under approximately 150 nm had nearly double the number of protofibrils compared to their uncross-linked counterpart. This observation is indicative of fiber compaction, which has been ascribed to cross-linking of the αC-regions that tether the protofibrils together [11].

Altogether, the imaging data show that the rFib340 and rFib420 fibrinogen variants form fibrin networks with a comparable fiber and network structure, except at 4 mg/mL, where rFib420 forms denser networks than rFib340. Structural differences between the networks can, therefore, not explain why the rFib420 networks are softer and more extensible than rFib340 networks over the whole range of 1 to 4 mg/mL fibrinogen.

3.3 | Shear-induced network remodeling

Having ruled out structural differences as a major factor to explain the mechanical differences between uncross-linked rFib420 and rFib340 networks, we returned to our hypothesis that the α_EC domain of rFib420 participates in fiber stretching. In case of uncross-linked fibrin, the fibers can lengthen via sliding of the constituent protofibrils [33,41]. Our observation that uncross-linked rFib420 networks

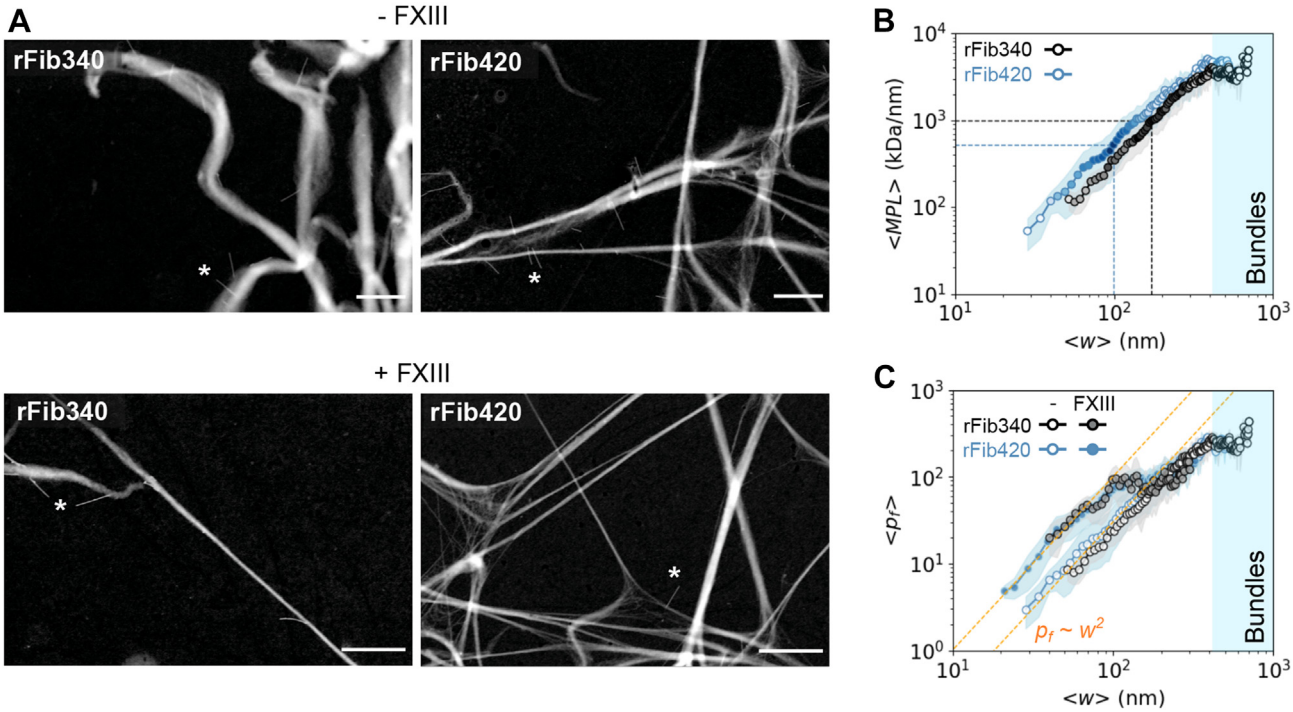

FIGURE 4 Impact of factor XIIIa cross-linking on fibrin fiber structure and packing density. (A) Scanning transmission electron microscopy images of fibrin layers transferred to electron microscopy grids from the inside of networks assembled in bulk at 1 mg/mL, with or without cross-linking by FXIIIa. The thin and short rods are *Tobacco mosaic virus* (indicated with an asterisk) used as internal mass calibration for mass mapping. Scale bar is 1 μm. (B) Mass per unit length (MPL) as a function of fiber width for uncross-linked recombinant human fibrinogen (rFib) 340 (in black) and rFib420 (in blue) networks. The values were extracted from scanning transmission electron microscopy images using a semiautomated fiber tracking algorithm [45]. The dotted lines indicate the mean width and MPL values. The scatter plot is color-coded with the percentage of transversal profiles per point, from 0 (white) to 100% (dark blue or black). The line shading represents the SD. Note that the curves flatten for large fiber widths because, in this regime, most analyzed segments are bundles of fibers. (C) The mean number of protofibrils (p_f) as a function of fiber diameter for fibrin networks with (filled circles) and without (hollow circles) FXIIIa cross-linking, obtained by normalizing the MPL data in Figure 4B by the MPL of a protofibril (14.4 kDa/nm for rFib340 and 17.8 kDa/nm for rFib420). The dashed orange lines indicate the scaling $p_f \propto w^2$ expected from a solid packed fiber.

are softer and more extensible than rFib340 networks hence suggests that the α_EC domain may facilitate protofibril sliding. To test this hypothesis, we investigated the stress response of rFib340 and rFib420 fibrin networks under repeated large-strain deformations. We were inspired by a study by Münster et al. [41], which showed by combining rheology and confocal imaging that uncross-linked fibrin fibers lengthen when fibrin networks are repeatedly strained.

Figure 5A shows the resulting stress-strain cycles of uncross-linked rFib340 and rFib420 networks formed at 2 mg/mL. We observed that in a series of cyclic deformations, the stress-strain curves continually shifted toward lower stress values in response to repeated loading. This means that repeated loading delays the occurrence of strain stiffening. Remarkably, all cycles could be collapsed onto a single master curve by rescaling each cycle with its characteristic strain γ_{char} (Figure 5C), defined as the strain value where the elastic stress σ_{el} (corresponding to the midpoint between the load and unload curves of each cycle) was equal to a threshold stress value, σ_{th}. This data rescaling indicates that the fibrin fibers undergo persistent lengthening upon repeated loading. As expected, the rFib420 networks show a higher shift in their characteristic strain within a series of cyclic deformations at fixed strain amplitude (Figure 5B). When comparing the values of γ_{char} at the last cycle before the networks start to rupture, the rFib420 networks show a shift in γ_{char} that is almost 2-fold larger than for rFib340 networks, supporting our hypothesis that the α_EC globular domain allows for an increased lengthening of the fibers. In contrast, upon cross-linking with FXIIIa, the stress-strain cycles for cross-linked networks of rFib340 and rFib420 no longer shifted (Figure 5D, E). This observation provides strong evidence that protofibril sliding is important for uncross-linked networks while it is prevented in cross-linked networks.

4 | DISCUSSION

The αC domain of fibrinogen has been the focus of several prior studies addressing the molecular origins of fibrin's remarkable mechanical behavior (reviewed by Medved and Weisel [56]). Theoretical models and experimental evidence show that the αC-region can impact the extensibility of fibrin fibers by facilitating protofibril sliding [33,34]. Here, we compared the structure and mechanics of rFib340 and rFib420 networks. The only difference in the molecular

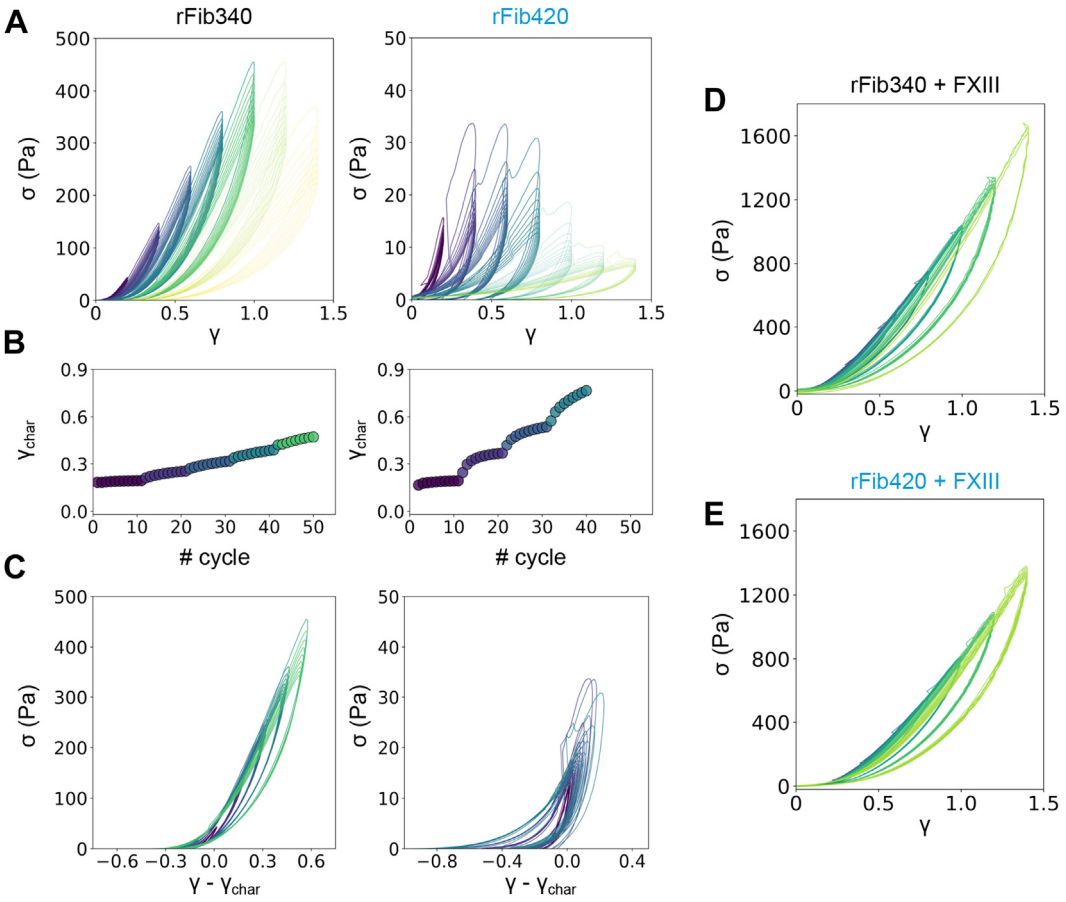

FIGURE 5 Viscoelastic response of recombinant human fibrinogen (rFib) 340 and rFib420 networks under repeated large-amplitude oscillatory strain. (A) Stress-to-strain response of uncross-linked 2 mg/mL rFib340 (left) and rFib420 (right) fibrin networks. In both cases, sets of 10 strain oscillations with stepwise increasing amplitude (20%-140%, in steps of 20%) are imposed. Each amplitude step is visualized with different colored curves. The dimmed curves correspond to the cycles after rupture. (B) Characteristic strain γ_{char} as a function of cycle number. (C) Rescaling of the stress-strain curves onto a single master curve by subtracting γ_{char} for each cycle. (D, E) Stress-to-strain response of 2 mg/mL rFib340 (D) and rFib420 (E) fibrin networks cross-linked with factor XIIIa.

structure between these variants was an extra globular domain at the αC-region present in fibrinogen-420 [25]. Structurally, fibrin networks from both variants were nearly identically formed at 1 to 2 mg/mL, while rFib420 networks were significantly denser than rFib340 networks at 4 mg/mL. This observation is consistent with previous reports that the α_EC domains hamper lateral association of protofibrils because they are arranged on the fiber surface [30]. This effect could be more visible on the 4 mg/mL networks due to a higher fibrinogen-thrombin ratio, where the low amount of free thrombin could facilitate the arrangement of the α_EC nodule to the fiber surface, effectively blocking lateral aggregation. Interestingly, we found striking differences in the mechanical behavior of fibrin networks formed from the 2 variants, but only in the absence of FXIIIa-mediated cross-linking. Uncross-linked rFib420 networks showed much higher extensibility than that shown by rFib340 networks, with the strain-stiffening regime being clearly different at strains larger than 20%.

Based on our findings, we propose that the interplay of αC-regions and FXIIIa cross-linking dictates the strain-stiffening response and the extensibility of fibrin networks with the following mechanism, schematized in Figure 6: while in the rFib340 variant, the αC-chains form a Velcro-like interaction between protofibrils, the α_EC domains, with their additional globular structure, prevent strong interactions between the αC-chains allowing for protofibrils to slide more easily upon fiber stretching. The reduced interaction between the α_EC domains and the easier movement of protofibrils result in larger extensibility for rFib420 fibrin networks. However, when FXIIIa cross-linking is added, it causes the fibers to compact by forming strong covalent bridges between the protofibrils, thus blocking any protofibril sliding and channeling the applied strain or stress directly along the structured fibrinogen domains, which form the protofibril backbone. Since the protofibril backbones are identical for the rFib340 and rFib420 variants, they show an identical network strain-stiffening response upon FXIIIa-mediated cross-linking. Interestingly, our results suggest that this effect is driven predominantly by γ–γ cross-linking since our samples show low levels of α-chain cross-linking (Supplementary Figure S3). While γ–γ cross-links occur within 30 minutes, α-chain cross-linking reaches high levels after 1 to 3 hours [11,31]; thus, our chosen incubation time of 90 minutes (where G_o

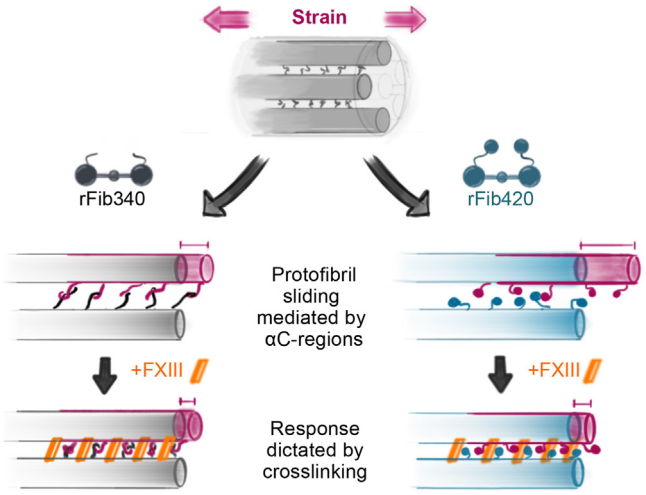

FIGURE 6 Interplay of αC-regions and factor XIIIa cross-linking in the strain stiffening of fibrin networks. Schematic representation of the suggested role for the αC-regions and the FXIIIa-mediated cross-linking in fibrin extensibility. For uncross-linked networks, the extensibility is mediated by the sliding of protofibrils, with recombinant human fibrinogen (rFib) 420 showing higher extensibility due to a low interaction of the α_EC domains. When fibrin is cross-linked by FXIIIa, protofibril sliding is inhibited, resulting in a similar strain-stiffening response for rFib340 and rFib420 networks.

reaches a plateau) is likely insufficient for complete α-chain cross-linking.

Our results show that the α_EC globular domains of fibrinogen strongly affect the structure and mechanics of fibrin networks, including the nonlinear regime and the rupture strain, which determines the ability of blood clots to withstand blood flow and internal platelet contractions [1]. Since fibrinogen-420 is more highly expressed in newborns than in adults [16], it is interesting to investigate whether there are any specific biomechanical functions of this variant during early childhood development. Intriguingly, recent work revealed a link between the extended Aα-chain and early hemostasis in young zebrafish [57], where rapid thrombosis upon laser injury suggests that the extended Aα-chain has a more effective coagulation response than the normal variant.

Since our results were obtained with 100% rFib420 clots, we cannot yet establish a direct link with its physiological role. Nevertheless, given the importance of the αC-chain in fibrin assembly, it is likely that low quantities of the α_EC variant will have a notable effect. For example, substituting the human αC-region with the analogous chicken domain can impact lateral aggregation of fibrinogen mixtures containing as little as 10% of the hybrid protein [58]. Hence, a systematic characterization of fibrinogen mixtures containing both variants, Fib340 and Fib420, could identify the significance of our findings in a physiological setting. Furthermore, the α_EC domain contains a binding site for integrins that mediate the recruitment of leukocytes to sites of inflammation [59], emphasizing the need for future studies on fibrin-cell interactions.

ACKNOWLEDGMENTS

C.M.-T. gratefully acknowledges financial support via a VENI grant from the Netherlands Organization for Scientific Research (grant number 680-47-462). This work was supported by funding from the European Union's Horizon Europe Research and Innovation Program (under grant agreement number 190183175) and research funding provided by Fibriant B.V. We thank A. Lof for assistance with scanning transmission electron microscopy imaging and J. -L. Pellequer for kindly gifting the tobacco mosaic virus rods.

AUTHOR CONTRIBUTIONS

C.M.-T., G.H.K., and J.K. conceptualized the study. C.M.-T. and J.G. performed the experiments. C.M.-T. performed data analysis. C.M.-T. and G.H.K. acquired funding. G.H.K. supervised the study. C.M.-T. performed visualizations. C.M.-T. wrote the original draft. All authors reviewed and edited the manuscript.

DECLARATION OF COMPETING INTERESTS

J.G. and J.K. are full-time employees of Fibriant B.V., Leiden. There are no other competing interests to disclose.

REFERENCES

[1] Litvinov RI, Weisel JW. Fibrin mechanical properties and their structural origins. *Matrix Biol*. 2017;60–61:110–23.
[2] Xu S, Xu Z, Kim OV, Litvinov RI, Weisel JW, Alber M. Model predictions of deformation, embolization and permeability of partially obstructive blood clots under variable shear flow. *J R Soc Interface*. 2017;14:20170441.
[3] Qiu Y, Myers DR, Lam WA. The biophysics and mechanics of blood from a materials perspective. *Nat Rev Mater*. 2019;4:294–311.
[4] Takeda Y. Studies of the metabolism and distribution of fibrinogen in healthy men with autologous 125-I-labeled fibrinogen. *J Clin Invest*. 1966;45:103–11.
[5] Kollman JM, Pandi L, Sawaya MR, Riley M, Doolittle RF. Crystal structure of human fibrinogen. *Biochemistry*. 2009;48:3877–86.
[6] Litvinov RI, Yakovlev S, Tsurupa G, Gorkun OV, Medved L, Weisel JW. Direct evidence for specific interactions of the fibrinogen αC-domains with the central E region and with each other. *Biochemistry*. 2007;46:9133–42.
[7] Protopopova AD, Litvinov RI, Galanakis DK, Nagaswami C, Barinov NA, Mukhitov AR, Klinov DV, Weisel JW. Morphometric characterization of fibrinogen's αC regions and their role in fibrin self-assembly and molecular organization. *Nanoscale*. 2017;9:13707–16.
[8] Fowler WE, Hantgan RR, Hermans J, Erickson HP. Structure of the fibrin protofibril. *Proc Natl Acad Sci U S A*. 1981;78:4872–6.
[9] Yeromonahos C, Polack B, Caton F. Nanostructure of the fibrin clot. *Biophys J*. 2010;99:2018–27.
[10] Hategan A, Gersh KC, Safer D, Weisel JW. Visualization of the dynamics of fibrin clot growth 1 molecule at a time by total internal reflection fluorescence microscopy. *Blood*. 2013;121:1455–8.
[11] Kurniawan NA, Grimbergen J, Koopman J, Koenderink GH. Factor XIII stiffens fibrin clots by causing fiber compaction. *J Thromb Haemost*. 2014;12:1687–96.
[12] Baradet TC, Haselgrove JC, Weisel JW. Three-dimensional reconstruction of fibrin clot networks from stereoscopic intermediate voltage electron microscope images and analysis of branching. *Biophys J*. 1995;68:1551–60.
[13] Ryan EA, Mockros LF, Weisel JW, Lorand L. Structural origins of fibrin clot rheology. *Biophys J*. 1999;77:2813–26.

[14] Schmitt LR, Henderson R, Barrett A, Darula Z, Issaian A, D'Alessandro A, Clendenen N, Hansen KC. Mass spectrometry–based molecular mapping of native FXIIIa cross-links in insoluble fibrin clots. *J Biol Chem*. 2019;294:8773–8.

[15] Klykov O, van der Zwaan C, Heck AJR, Meijer AB, Scheltema RA. Missing regions within the molecular architecture of human fibrin clots structurally resolved by XL-MS and integrative structural modeling. *Proc Natl Acad Sci U S A*. 2020;117:1976, 87.

[16] Grieninger G, Lu X, Cao Y, Fu Y, Kudryk BJ, Galanakis DK, Hertzberg KM. Fib420, the novel fibrinogen subclass: newborn levels are higher than adult. *Blood*. 1997;90:2609–14.

[17] Holm B, Godal HC. Quantitation of the three normally-occurring plasma fibrinogens in health and during so-called "acute phase" by SDS electrophoresis of fibrin obtained from EDTA-plasma. *Thromb Res*. 1984;35:279–90.

[18] Holm B, Nilsen DW, Kierulf P, Godal HC. Purification and characterization of 3 fibrinogens with different molecular weights obtained from normal human plasma. *Thromb Res*. 1985;37:165–76.

[19] Nieuwenhuizen W. Biochemistry and measurement of fibrinogen. *Eur Heart J*. 1995;16:6–10.

[20] Collet JP, Moen JL, Veklich YI, Gorkun OV, Lord ST, Montalescot G, Weisel JW. The αC domains of fibrinogen affect the structure of the fibrin clot, its physical properties, and its susceptibility to fibrinolysis. *Blood*. 2005;106:3824–30.

[21] Kaijzel EL, Koolwijk P, van Erck MGM, van Hinsbergh VWM, de Maat MPM. Molecular weight fibrinogen variants determine angiogenesis rate in a fibrin matrix in vitro and in vivo. *J Thromb Haemost*. 2006;4:1975–81.

[22] Weijers EM, van Wijhe MH, Joosten L, Horrevoets AJG, de Maat MPM, van Hinsbergh VWM, Koolwijk P. Molecular weight fibrinogen variants alter gene expression and functional characteristics of human endothelial cells. *J Thromb Haemost*. 2010;8:2800–9.

[23] McPherson HR, Duval C, Baker SR, Hindle MS, Cheah LT, Asquith NL, Domingues MM, Ridger VC, Connell SD, Naseem KM, Philippou H, Ajjan RA, Ariens RA. Fibrinogen αC-subregions critically contribute blood clot fibre growth, mechanical stability, and resistance to fibrinolysis. *eLife*. 2021;10:e68761.

[24] Chung DW, Davie EW. Gamma and gamma' chains of human fibrinogen are produced by alternative mRNA processing. *Biochemistry*. 1984;23:4232–6.

[25] Fu Y, Grieninger G. Fib420: a normal human variant of fibrinogen with two extended alpha chains. *Proc Natl Acad Sci U S A*. 1994;91:2625–8.

[26] Spraggon G, Applegate D, Everse SJ, Zhang JZ, Veerapandian L, Redman C, Doolittle RF, Grieninger G. Crystal structure of a recombinant αEC domain from human fibrinogen-420. *Proc Natl Acad Sci U S A*. 1998;95:9099–104.

[27] Fu Y, Weissbach L, Plant PW, Oddoux C, Cao Y, Liang TJ, Roy SN, Redman CM, Grieninger G. Carboxy-terminal-extended variant of the human fibrinogen α subunit: a novel exon conferring marked homology to β and γ subunits. *Biochemistry*. 1992;31:11968–72.

[28] Fu Y, Zhang JZ, Redman CM, Grieninger G. Formation of the human fibrinogen subclass fib420: disulfide bonds and glycosylation in its unique (αE chain) domains. *Blood*. 1998;92:3302–8.

[29] Applegate D, Haraga L, Hertzberg KM, Steben LS, Zhang JZ, Redman CM, Grieninger G. The α_EC domains of human fibrinogen$_{420}$ contain calcium binding sites but lack polymerization pockets. *Blood*. 1998;92:3669–74.

[30] Mosesson MW, DiOrio JP, Hernandez I, Hainfeld JF, Wall JS, Grieninger G. The ultrastructure of fibrinogen-420 and the fibrin-420 clot. *Biophys Chem*. 2004;112:209–14.

[31] Applegate D, Steben LS, Hertzberg KM, Grieninger G. The αEC domain of human fibrinogen-420 is a stable and early plasmin cleavage product. *Blood*. 2000;95:2297–303.

[32] Tang H, Fu Y, Zhan S, Luo Y. α_EC, the C-terminal extension of fibrinogen, has chaperone-like activity. *Biochemistry*. 2009;48:3967–76.

[33] Houser JR, Hudson NE, Ping L, O'Brien ET, Superfine R, Lord ST, Falvo MR. Evidence that αC region is origin of low modulus, high extensibility, and strain stiffening in fibrin fibers. *Biophys J*. 2010;99:3038–47.

[34] Falvo MR, Millard D, O'Brien ET, Superfine R, Lord ST. Length of tandem repeats in fibrin's αC region correlates with fiber extensibility. *J Thromb Haemost*. 2008;6:1991, 3.

[35] Vos BE, Martinez-Torres C, Burla F, Weisel JW, Koenderink GH. Revealing the molecular origins of fibrin's elastomeric properties by in situ X-ray scattering. *Acta Biomater*. 2020;104:39–52.

[36] Wang Y, Kumar S, Nisar A, Bonn M, Rausch MK, Parekh SH. Probing fibrin's molecular response to shear and tensile deformation with coherent Raman microscopy. *Acta Biomater*. 2021;121:383–92.

[37] Kumar S, Wang Y, Hedayati M, Fleissner F, Rausch MK, Parekh SH. Structural control of fibrin bioactivity by mechanical deformation. *Proc Natl Acad Sci U S A*. 2022;119:e2117675119.

[38] de Maat MPM, Verschuur M. Fibrinogen heterogeneity: inherited and noninherited. *Curr Opin Hematol*. 2005;12:377–83.

[39] Smith EL, Cardinali B, Ping L, Ariëns RA, Philippou H. Elimination of coagulation factor XIII from fibrinogen preparations. *J Thromb Haemost*. 2013;11:993–5.

[40] Kurniawan NA, Vos BE, Biebricher A, Wuite GJ, Peterman EJ, Koenderink GH. Fibrin networks support recurring mechanical loads by adapting their structure across multiple scales. *Biophys J*. 2016;111:1026–34.

[41] Münster S, Jawerth LM, Leslie BA, Weitz JI, Fabry B, Weitz DA. Strain history dependence of the nonlinear stress response of fibrin and collagen networks. *Proc Natl Acad Sci U S A*. 2013;110:12197–202.

[42] Schneider CA, Rasband WS, Eliceiri KW. NIH Image to ImageJ: 25 years of image analysis. *Nat Methods*. 2012;9:671–5.

[43] Macrae FL, Duval C, Papareddy P, Baker SR, Yuldasheva N, Kearney KJ, McPherson HR, Asquith N, Konings J, Casini A, Degen JL, Connell SD, Philippou H, Wolberg AS, Herwald H, Ariëns RA. A fibrin biofilm covers blood clots and protects from microbial invasion. *J Clin Invest*. 2018;128:3356–68.

[44] Müller SA, Engel A. Structure and mass analysis by scanning transmission electron microscopy. *Micron*. 2001;32:21–31.

[45] Martinez-Torres C, Burla F, Alkemade C, Koenderink GH. Revealing the assembly of filamentous proteins with scanning transmission electron microscopy. *PLoS One*. 2019;14:e0226277.

[46] Brown AE, Litvinov RI, Discher DE, Purohit PK, Weisel JW. Multiscale mechanics of fibrin polymer: gel stretching with protein unfolding and loss of water. *Science*. 2009;325:741–4.

[47] Fleissner F, Bonn M, Parekh SH. Microscale spatial heterogeneity of protein structural transitions in fibrin matrices. *Sci Adv*. 2016;2:e1501778.

[48] Piechocka IK, Bacabac RG, Potters M, MacKintosh FC, Koenderink GH. Structural hierarchy governs fibrin gel mechanics. *Biophys J*. 2010;98:2281–9.

[49] Weigandt KM, Porcar L, Pozzo DC. In situ neutron scattering study of structural transitions in fibrin networks under shear deformation. *Soft Matter*. 2011;7:9992.

[50] Piechocka IK, Jansen KA, Broedersz CP, Kurniawan NA, MacKintosh FC, Koenderink GH. Multi-scale strain-stiffening of semiflexible bundle networks. *Soft Matter*. 2016;12:2145–56.

[51] Brown AE, Litvinov RI, Discher DE, Weisel JW. Forced unfolding of coiled-coils in fibrinogen by single-molecule AFM. *Biophys J*. 2007;92:L39–41.

[52] Litvinov RI, Faizullin DA, Zuev YF, Weisel JW. The α-helix to β-sheet transition in stretched and compressed hydrated fibrin clots. *Biophys J*. 2012;103:1020–7.

[53] Averett RD, Menn B, Lee EH, Helms CC, Barker T, Guthold M. A modular fibrinogen model that captures the stress-strain behavior of fibrin fibers. *Biophys J*. 2012;103:1537–44.

[54] Helms CC, Ariëns RA, Uitte de Willige S, Standeven KF, Guthold M. α–α Cross-links increase fibrin fiber elasticity and stiffness. *Biophys J*. 2012;102:168–75.

[55] Guthold M, Liu W, Stephens B, Lord ST, Hantgan RR, Erie DA, Taylor R, Superfine R. Visualization and mechanical manipulations of individual fibrin fibers suggest that fiber cross section has fractal dimension 1.3. *Biophys J*. 2004;87:4226–36.

[56] Medved L, Weisel JW. The story of the fibrin(ogen) αC-domains: evolution of our view on their structure and interactions. *Thromb Haemost*. 2022;122:1265–78.

[57] Freire C, Fish RJ, Vilar R, Di Sanza C, Grzegorski SJ, Richter CE, Shavit JA, Neerman-Arbez M. A genetic modifier of venous thrombosis in zebrafish reveals a functional role for fibrinogen AαE in early hemostasis. *Blood Adv*. 2020;4:5480–91.

[58] Ping L, Huang L, Cardinali B, Profumo A, Gorkun OV, Lord ST. Substitution of the human αC region with the analogous chicken domain generates a fibrinogen with severely impaired lateral aggregation: fibrin monomers assemble into protofibrils but protofibrils do not assemble into fibers. *Biochemistry*. 2011;50:9066–75.

[59] Lishko VK, Yakubenko VP, Hertzberg KM, Grieninger G, Ugarova TP. The alternatively spliced αEC domain of human fibrinogen-420 is a novel ligand for leukocyte integrins αMβ2 and αXβ2. *Blood*. 2001;98:2448–55.

SUPPLEMENTARY MATERIAL

The online version contains supplementary material available at https://doi.org/10.1016/j.jtha.2023.10.025